Wide-band precision rectification

C. Toumazou, BSc, PhD
F.J. Lidgey, BSc, PhD, CEng, MIEE

Indexing terms: Amplifiers, Convertors, Circuit theory and design, Power conversion

Abstract: Operational-amplifier supply-current sensing is employed in the design of high-performance precision rectification. The designs presented in this paper compare favourably with conventional precision rectifier circuits both in linearity and bandwidth, and are constructed from low supply bias-current operational amplifiers and current mirrors. Application of this new rectifying technique in the design of precision peak-detector circuits is also described.

1 Introduction

Traditional designs of precision rectifier circuits are usually some arrangement of operational amplifiers, diodes and resistors [1–5]. The most popular scheme of a precision full-wave rectifier is that shown in Fig. 1. The

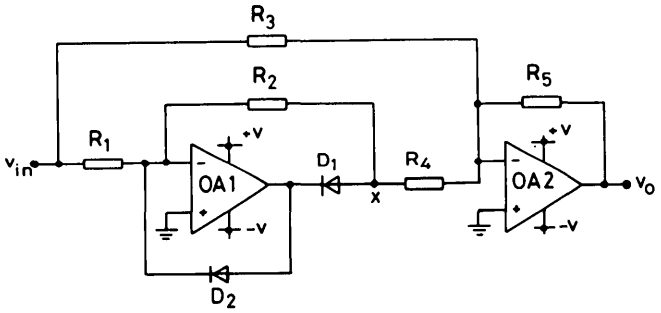

Fig. 1 *Conventional precision full-wave rectifier*
$R_1 = R_2 = R_3 = R_5 = R$
$R_4 = R/2$

circuit will produce an output voltage V_0 which is the full-wave rectified version of an alternating input waveform applied at V_{in}. Half-wave rectification of the input is obtained by taking an output at node (x) on the circuit. Although this scheme is attractive in that it minimises the effect of the diode voltage drop across D_1, when in its forward conducting mode it suffers from two major disadvantages:

(i) During the crossover from positive to negative input polarity, operational amplifier OA1 does not remain in its linear active mode. The transition time during which OA1 is open loop results in undesirable output-signal distortion at relatively low frequencies.

(ii) If precise signal rectification between input and output is to be obtained, the use of closely matched resistors is essential.

Paper 5086G (E10), first received 24th March and in revised form 18th September 1986

Dr. Lidgey is, and Dr. Toumazou was formerly, with the Department of Engineering, Oxford Polytechnic, Headington, Oxford OX3 0BP, United Kingdom

Dr. Toumazou is now with the Department of Electrical Engineering, Imperial College of Science and Technology, London SW7 2AZ, United Kingdom

The authors have evaluated the circuit of Fig. 1 using several different types of operational amplifier in an attempt to obtain the best performance. However, results have shown significant output-signal distortion to occur, in most cases at frequencies well below the full-power frequency capabilities of the operational amplifier used.

Several alternative schemes, reported in the late 1970s [6–8], can provide precision rectification without the use of diodes in the circuit. For example, in the proposed single-transistor full-wave rectifier [7], reasonably high-frequency performance can be obtained, at the expense of poor output-signal linearity for low-amplitude inputs. Perhaps the most versatile of these schemes is the one proposed by Barker and Hart [6]. Two complementary push-pull amplifiers together with two operational amplifiers are arranged to provide precision full-wave rectification. However, the class-B mode in which this circuit operates imposes similar frequency limits to those rectifiers that employ diodes in their circuits.

The circuits described in this paper use operational-amplifier supply-current sensing to obtain accurate phase splitting of the input signal. The precision rectifiers obtained using this technique are particularly attractive in that they provide high performance at low cost.

2 Circuit principle

Operational-amplifier supply-current sensing is a technique widely used in the design of current-converter [9–14] and current-conveyer [15–17] circuits. This technique is particularly useful since, for most operational amplifiers, it is not possible to gain access to their output current independently. Current mirrors are used to sense the phase-split output current via the supply leads to the operational amplifier. The current-mirror outputs are then recombined to produce a single bipolar output. To obtain a unipolar output, a similar structure is adopted with the current-mirror outputs appropriately recombined to produce either half- or full-wave precision rectification, as shown in Fig. 2.

3 Circuit description

A precision positive half-wave rectifier is shown in Fig. 2*a*. The circuit comprises essentially two operational amplifiers OA1 and OA2, and two current mirrors CM1 and CM2. Wilson's [12] current-mirror symbol has been used to simplify the diagram. OA1 is connected as a voltage-to-current converter at the input side of the circuit and OA2 as a current-to-voltage converter at the output. For a first-order description of the circuit assume both operational amplifiers to be ideal. With V_{in} set at zero, positive supply current I_1 is reflected to current-output node (x) by the action of current mirror CM1. Bias current I_2, provided by current-mirror sink CM2 and resistance R_p, is nominally set equal to I_1, then appropriately adjusted until current I_x and, therefore,

output voltage V_0 are also set equal to zero. The circuit is now in a state of balance. Current mirrors CM1 and CM2 should be a similar type to provide circuit symmetry at node (x).

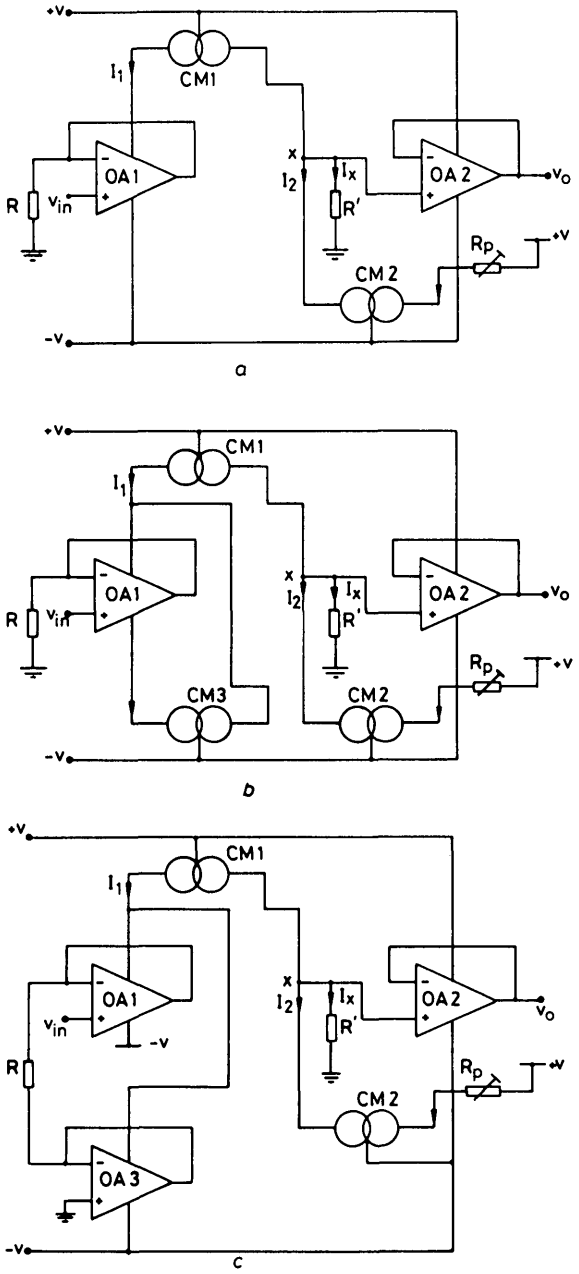

Fig. 2 *Proposed rectifier circuits*
a Precision positive half-wave rectifier
b Precision full-wave rectifier
c Improved precision full-wave rectifier

For $V_{in} > 0$, positive supply current I_1 will now increase by approximately V_{in}/R; this will cause I_x to increase by a similar amount and V_0 to become approximately equal to $V_{in}R'/R$. For a precise unity-gain voltage transfer between input and output, current mirror CM1 must have almost ideal current-transfer properties and resistor R' must be very well matched to R. However, as the function of R' is solely to provide current-to-voltage conversion at the circuits output, it may be made adjustable, and provide sufficient scaling to prevent current-mirror inaccuracies in CM1 from affecting the circuit precision.

For $V_{in} < 0$, input current V_{in}/R is drawn by the negative supply rail of OA1. The output of the circuit is unaffected by this action and, therefore, I_x and V_0 will remain equal to zero. The net result is an output signal equal in magnitude to the half-wave rectified version of the input signal.

Full-wave rectification of the input signal is achieved by the addition of current mirror CM3, shown in Fig. 2*b*. CM3 is used to sense OA1's negative output current during the input condition $V_{in} < 0$. By connecting the output of current mirror CM3 to the input of current mirror CM1 as shown, an in-phase addition of both OA1's positive and negative output-signal current is obtained. As a result V_0 will now become proportional to the absolute value of V_{in} and, therefore, provide a full-wave rectification of the input signal. Note that further adjustment of bias current I_2 is necessary to compensate for the increase in bias current now flowing through current mirror CM1.

However, this scheme suffers from one major drawback: over the complete positive and negative input cycle there is a difference between the number of current-mirror signal paths seen by the output. This implies that if V_0 is to accurately represent the absolute value of V_{in}, current mirrors CM1 and CM3 must perform with almost ideal current-transfer properties. The overall accuracy of this circuit is, therefore, dependent upon the quality of the current mirrors used.

To overcome this current-mirror dependence in circuit performance, current mirror CM3 is replaced with operational amplifier OA3 as shown in Fig. 2*c*. OA1 and OA3 now combine to form a differential voltage-to-current converter at the input of the circuit. For $V_{in} > 0$, a differential current of V_{in}/R will flow through the positive supply rail of OA1 and the negative supply rail of OA3. As the input polarity is reversed, the opposite will occur and the operation of OA3 is now similar to that of current mirror CM3 described in the previous circuit. The two split phases then recombine at the input of current mirror CM1 and are converted to an output voltage by the action of CM1, R' and OA3 as previously described. Current-mirror sink CM2 is still employed in the circuit to provide the necessary bias-current cancellation at output node (x).

This configuration of a full-wave rectifier is particularly attractive as the signal current I_x has to pass through only one current-mirror path during both positive and negative input polarities. The current-transfer performance of current mirror CM1 is no longer a critical circuit parameter, as scaling for current-mirror inaccuracies can be provided by resistor R', as in the half-wave rectifier design of Fig. 2*a*.

In general, the main advantage of this new rectifying scheme over the more conventional type (Fig. 1) is that the operational amplifiers are always maintained in a closed loop, independent of input-signal polarity. The undesirable output-signal distortion predominant in most other designs is, therefore, totally eliminated with this new scheme. Also, by virtue of the total negative feedback, precision signal rectification can be performed up to frequencies principally determined by the −3 dB unity-gain bandwidth of the particular operational amplifiers used.

4 Practical considerations

In the rectifier-circuit description in Section 3, the operational amplifiers were assumed to be ideal. However, DC output offset arising from the operational-amplifier non-idealities, such as nonzero-input bias current and input-offset errors, can simply be nulled during the initial

zero-input/zero-output setting up procedure of the circuit, obviating the need for additional offset-nulling circuitry and low-input bias-current operational amplifiers.

A further assumption made during the circuit descriptions of Fig. 2 was that the input-signal current V_{in}/R was drawn from either the positive or negative supply rail, depending upon the input-signal polarity. However, this is not strictly true unless the magnitude of V_{in}/R is much greater than the quiescent bias current I_s flowing through the class-AB output stage of the operational amplifier. This should pose no problem as the maximum current-drive and current-sink capabilities of most operational amplifiers with a class-AB output stage are usually much greater than I_s, the only limitation being the maximum output current $\hat{I}_{out}$ set by the short-circuit protection network of the particular operational amplifier employed. For values of $|V_{in}/R|$ of the order of I_s, the current distribution in the operational amplifier's supply rails becomes nonlinear. This is because of the transition between class-A and class-AB behaviour of the operational amplifier's output stage at low current levels. The performance of current-converter circuits [9–14], based upon this principle, is unaffected by this low-signal operation, as the two unequally split portions of the input signal flowing through the operational amplifier's supply leads are summed at a single bipolar output; accurate reproduction of the input signal is, therefore, obtained at the converter's output. However, as the performance of the rectifier circuits described here relies upon the unipolar operation obtained from single supply-rail current sensing, nonlinear output performance will occur at these low-input current levels. For optimum rectifier performance, resistor R must, therefore, be chosen to satisfy the condition

$$\hat{I}_{out} > |V_{in}/R| \gg I_s \quad (1)$$

which suggests that operational amplifiers having a high $\hat{I}_{out}/I_s$ ratio are preferable.

To illustrate this, the rectifier circuit of Fig. 2c was constructed from two types of operational amplifier. In the first case LM741 operational amplifiers were used for OA1, OA2 and OA3. The operational amplifiers' supply bias current was measured to be 0.88 mA with maximum output current $\hat{I}_{out}$ of 14 mA. Operational amplifiers OA1 and OA3 were then replaced with LF441 low-power JFET operational amplifiers. With this operational amplifier the supply bias current was 0.14 mA and the maximum output current was 11 mA. I_s for both operational-amplifier types was about 25% of the supply bias current (see Appendix 10.2). The LM741 and LF441 have almost the same frequency response.

In each circuit the improved four-transistor Wilson [18] current mirrors, constructed from CA3096AE mixed-transistor arrays, were employed. This particular current mirror was chosen for its accurate current-transfer properties and high output impedance. The input impedance of the current mirror can, however, also be quite high, especially at very low bias-current levels. This is undesirable, as small signal voltages can develop at the operational amplifier's supply leads which may degrade the rectifier's performance, unless the power-supply rejection ratios of the operational amplifiers that are used are sufficiently high. The guaranteed power-supply rejection ratios for the LM741 and LF441 are in the range 90–100 dB; sufficiently high so that this effect is negligible.

5 Experimental results

5.1 Static characteristics

Fig. 3 shows plots of the transfer curves of the rectifier of Fig. 2c, obtained from a digital-storage oscilloscope with x-y plotting facilities.

The transfer curves shown in Figs. 3a and b were obtained using the LF441 operational amplifiers in the circuit, and in Figs. 3c and d using the LM741 operational amplifiers. In each case resistor R was chosen to be 10 Ω. Resistor R', nominally set equal to R, was adjusted to provide precise unity voltage transfer between the input and output of the rectifier. This low resistance was selected to demonstrate the rectifiers' performance for input signals in the millivolt range. However, rectification at higher input levels is obtained by increasing the value of R appropriately. The required bias-current cancellation at the rectifier's output was ensured by nominally setting bias current I_2 approximately equal to supply current I_1 and then appropriately adjusting R_p to obtain a zero output voltage V_0 for V_{in} set to zero. With a power-supply voltage V, of 15 V, the required value of R_p was 15.3 kΩ for LM741 operational amplifiers and 95.5 kΩ for the LF441 operational amplifiers.

Good linearity is seen in the transfer curves of both Fig. 3a and Fig. 3c, up to the value of V_{in} which causes the operational amplifier to current limit. However, it is evident that in the case of the LF441-based rectifier a much sharper and, therefore, more accurate transfer is obtained at lower input levels. This is shown clearly in the magnified transfer curves of Fig. 3b and Fig. 3d. Viewed on this higher-sensitivity voltage scale, the transfer curve of the LF441-based rectifier is evidently much sharper than in the equivalent 741-based structure. For values of V_{in} of about 5 mV, the transfer curve of Fig. 3d becomes severely nonlinear, due to the previously described change-over effect from class A to class AB in the operational amplifiers' output stage, expected here at values of V_{in} of the order of $I_s R \simeq 2.5$ mV. As I_s is lower in the LF441 operational amplifier, this results in better linearity shown in Fig. 3b at lower input levels. Nonlinear performance does occur, however, but now at values of V_{in} of about 0.5 mV, expected with an I_s of 0.036 mA (i.e. $I_s R \simeq 0.36$ mV).

The relatively inferior performance of the LM741-based rectifier can be seen in Fig. 4. The traces shown were obtained from the rectifier of Fig. 2c, employing (a) the LM741 operational amplifier, and (b) the LF441 operational amplifier. In each case the input-signal frequency was set to 10 kHz, at approximate input amplitudes of (i) 60 mV peak, and (ii) 6 V peak. For each input signal the value of R was chosen to satisfy the relation, expr. 1 and, therefore, provide the best rectifying performance, without current limiting the particular operational amplifier used. In addition to demonstrating the superior rectifying performance obtained with low supply-current operational amplifiers, the results demonstrate the circuit's ability to accommodate a wide range of signal amplitudes by simply varying resistor R.

Similar tests were performed on the half-wave rectifier of Fig. 2a, and the full-wave rectifier of Fig. 2b. Again, the best results were obtained using the low-power JFET operational amplifier in the circuit. The overall performance of the full-wave rectifier of Fig. 2b was, however, not as good as that of the rectifier of Fig. 2c, mainly because of the limitations described in Section 3.

Because the small-signal performance of the rectifier circuits described is dependent upon the behaviour of the

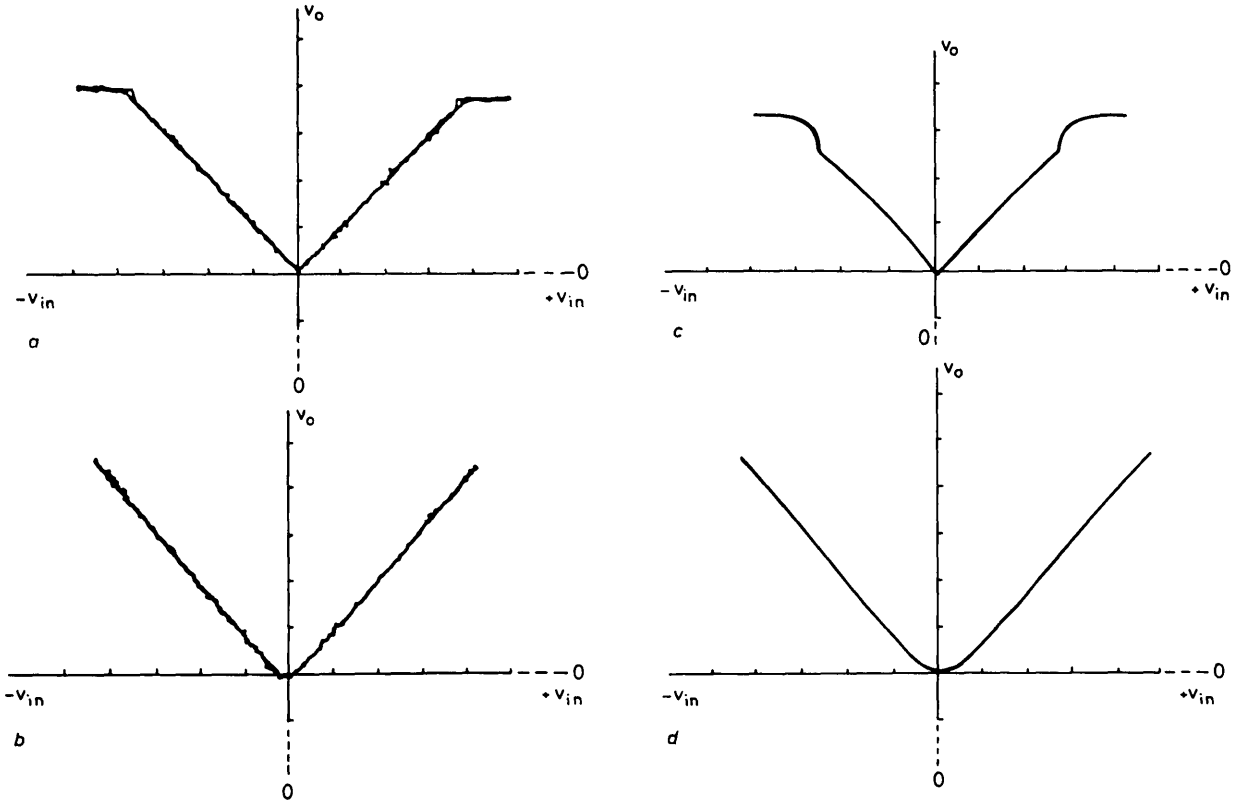

Fig. 3 *Transfer curves of improved precision full-wave rectifier*

a, b LF441 operational amplifier
c, d LM741 operational amplifier
a V_o, V_{in}: 30 mV/division
b V_o, V_{in}: 5 mV/division
c V_o, V_{in}: 50 mV/division
d V_o, V_{in}: 10 mV/division

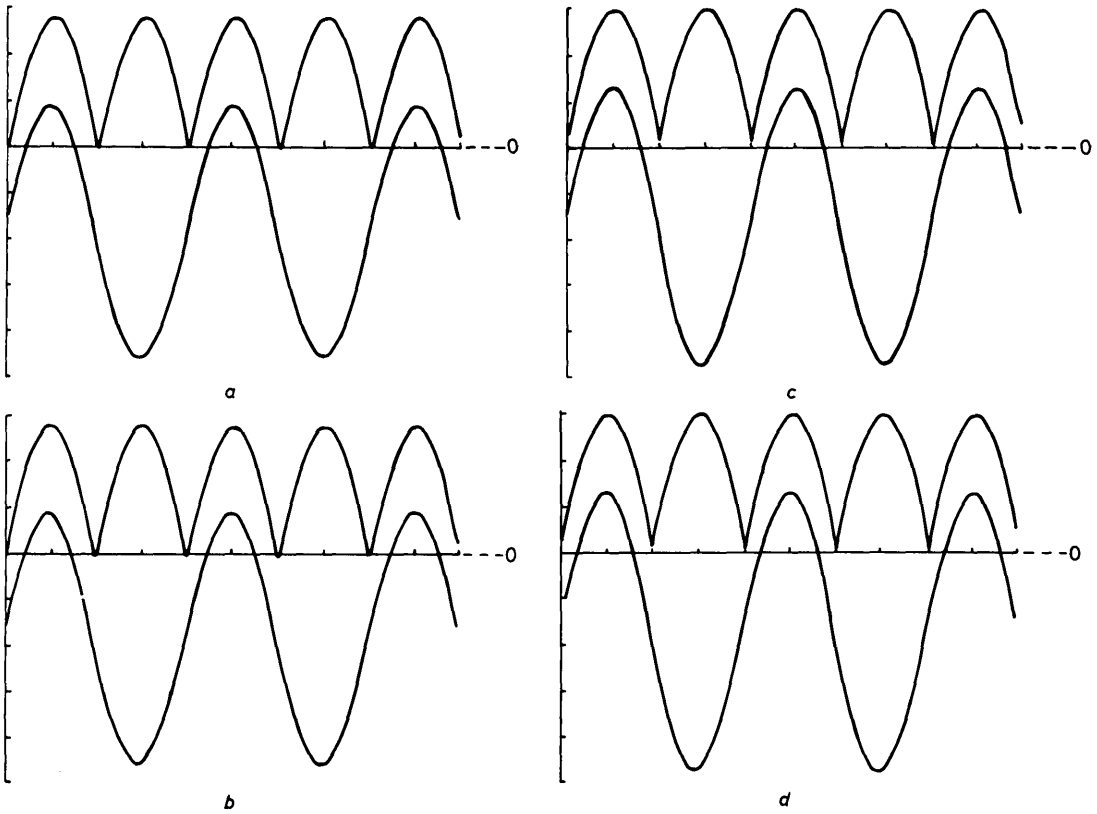

Fig. 4 *Rectifying characteristics of improved precision full-wave rectifier*

Lower traces: input; upper traces: output
Horizontal scale: 0.025 ms/division

a $R = 5\,\Omega$
Vertical scale: 20 mV/division
b $R = 500\,\Omega$
Vertical scale: 2 V/division

c $R = 10\,\Omega$
Vertical scale: 20 mV/division
d $R = 1\,k\Omega$
Vertical scale: 2 V/division

output stage of the operational amplifier as it is transferred from class A to class AB to class B, theoretical and experimental tests were carried out to establish the exact nature of this transition and the results are shown in Appendix 10.1.

5.2 High-frequency performance

To demonstrate the improved high-frequency behaviour possible with this new rectifying scheme, a comparison was made between the frequency performance of the conventional precision full-wave rectifier of Fig. 1, and the rectifier of Fig. 2c. The circuit of Fig. 1 was constructed for high performance, using, as recommended in Reference 4, LM308 operational amplifiers for OA1 and OA2 together with 50 pF compensation capacitors, connected in a feedforward configuration. This compensation is used to provide the amplifier with an expected small-signal bandwidth of up to 10 MHz. R_1, R_2, R_3 and R_5 were well matched 20 kΩ resistors and R_4 was an 11 kΩ variable resistor. R_4 was made adjustable to provide an accurate unity voltage gain. Diodes D_1 and D_2 were small-signal silicon diodes.

The rectifier circuit of Fig. 2c was constructed also using LM308 operational amplifiers. As this operational amplifier features a low supply bias current it is, therefore, particularly suitable to illustrate the advantages of the circuit of Fig. 2c over that of Fig. 1. In the circuit of Fig. 2c, resistors $R \simeq R'$ were set to 100 Ω, to obtain optimum signal-rectifying performance at the particular input-signal level used in this experiment. Resistor R_p was set to 50 kΩ to ensure the required zero-offset condition at the rectifiers output. As before, improved Wilson [18] current mirrors were used for CM1 and CM2. In both rectifier circuits a power-supply voltage of ±15 V was used.

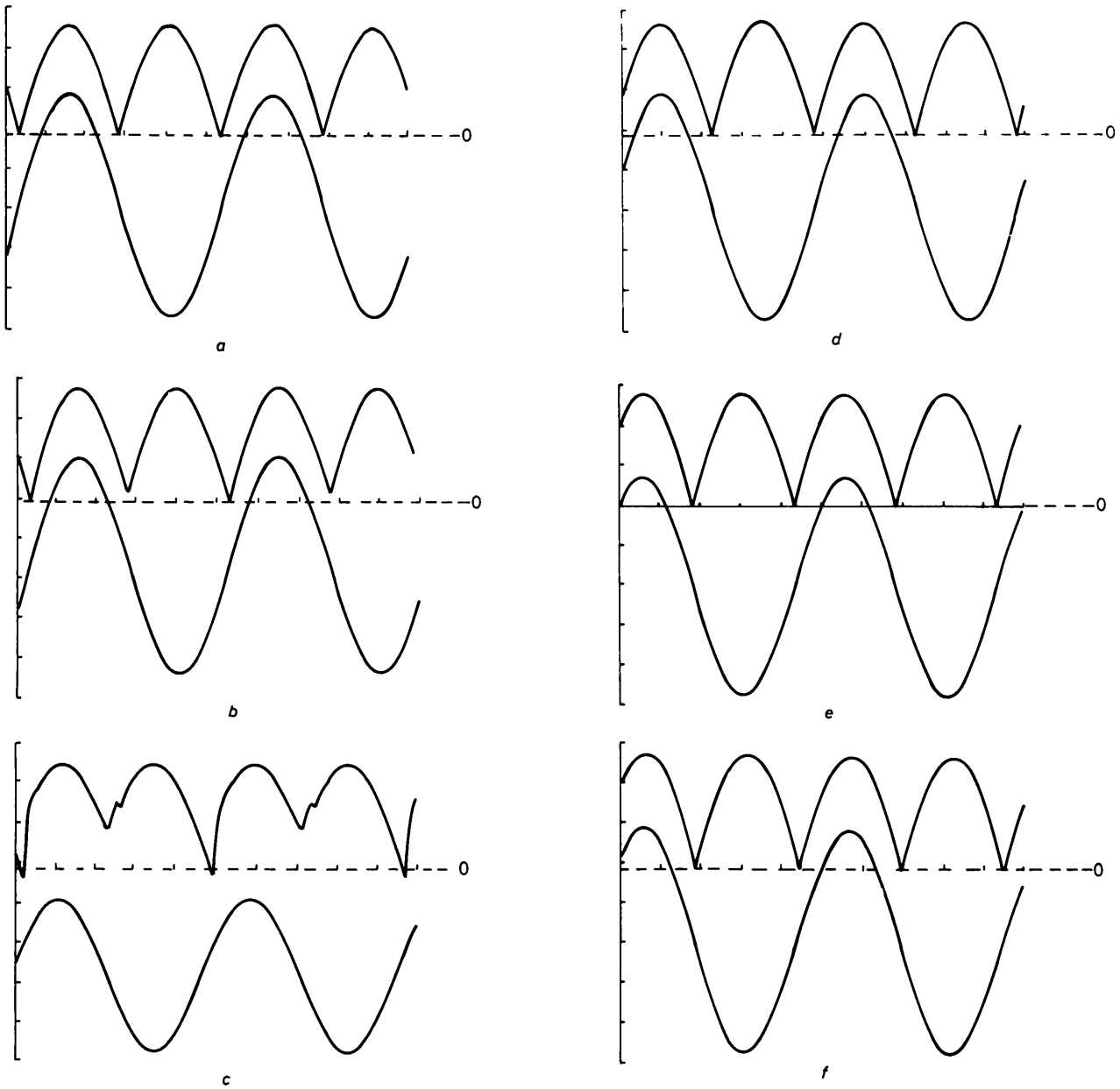

Fig. 5 *Comparative performance rectifier of Fig. 1 and rectifier of Fig. 2c*

Lower traces: input; upper traces: output
Vertical scale: 0.2 V/division
a, b, c Rectifier of Fig. 1
d, e, f Rectifier of Fig. 2c
a, d Horizontal scale: 2 ms/division
b, e Horizontal scale: 0.2 ms/division
c, f Horizontal scale: 0.02 ms/division

Input and output traces obtained from the two rectifiers are shown in Fig. 5*a* and Fig. 5*b* respectively. In each case, the input-signal amplitude was set to about 0.5 V peak, and the input frequency varied from 100 Hz to 10 kHz. At an input frequency of 100 Hz, the output signals shown in Figs. 5*a*(i) and 5*b*(i) are both accurate and linear. However, at a frequency of 1 kHz the output signal shown in Fig. 5*a*(ii), starts to distort and at 10 kHz becomes very distorted, as shown in Fig. 5*a*(iii). Equivalent output signals to these, shown in Fig. 5*b*(i) and Fig. 5*b*(ii), obtained from the new rectifying circuit of Fig. 2*c* are evidently much more linear at the same input-frequency values. In fact, further tests showed the rectifier to perform well up to a frequency of approximately 1 MHz; this limit being principally determined by the short fall in the frequency performance of the lateral *pnp* transistor arrays used to construct current mirror CM1.

6 Additional precision rectifier circuits

With the versatility of this new rectifying scheme, a number of variations to the circuits shown in Fig. 2 can be developed. For example, by reversing the polarity of current mirrors CM1 and CM2 in the circuit of Fig. 2*a*, as shown in Fig. 6*a*, negative half-wave rectification of

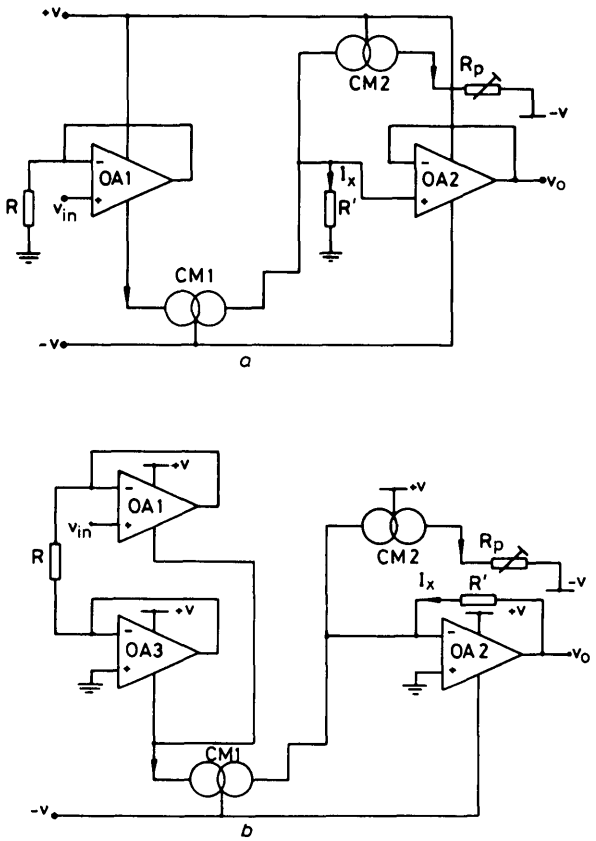

Fig. 6 *Alternative rectifiers*
a Precision negative half-wave rectifier
b Alternative precision full-wave rectifier

the input signal is now obtained. To provide this circuit and the rectifying circuits of Fig. 2 with output phase inversion, operational amplifier OA2 and resistor R' can be connected as an inverting transresistance amplifier. Using the above circuit modifications the precision full-wave rectifier circuit of Fig. 2*c* can be redesigned as shown in Fig. 6*b*. This alternative full-wave rectifier design is particularly attractive since performance limiting, lateral *pnp* transistors are no longer employed in the signal path.

7 Precision peak-detector design

As with the conventional precision rectifying circuits, conventional precision peak detectors [19] suffer from high-performance limitations, principally because of the operational amplifier switching between the hold and sample mode. The precision rectifying technique described in this paper can be similarly applied to provide high-performance precision peak detection.

The basic design of a precision positive peak detector is shown in Fig. 7. As before, low bias supply current

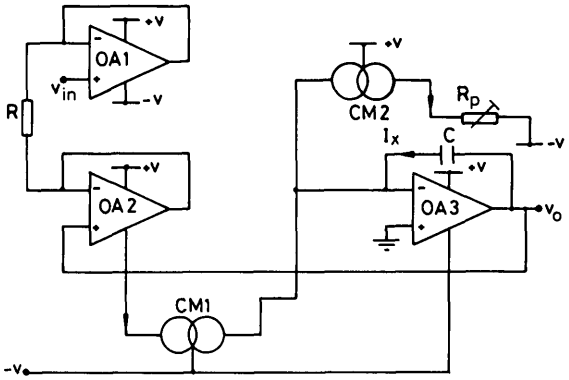

Fig. 7 *Precision positive peak detector*

operational amplifiers should be used. The circuit is connected as a positive half-wave rectifier. For $V_{in} > 0$, signal current $i_x = (V_{in} - v_0)/R$ will charge capacitor C until $V_{in} = V_0$ and $i_x = 0$. If V_{in} is now reduced, the signal current i_x is steered in the opposite direction and capacitor C continues to hold the peak value of V_{in}.

Optimum acquisition performance of the circuit is obtained by setting resistor R equal to zero. The circuit's acquisition rate for this condition will be $[\hat{I}_{out}/C]$ where $\hat{I}_{out}$ is the maximum output current provided by the first operational amplifier to current limit. However, as with all precision peak-detector circuits employing operational amplifiers, the dynamic-response limitations of the operational amplifier will limit the overall speed of the signal that can be processed.

Variations of precision peak-detector circuits can be made by simple modifications to the circuit of Fig. 7. For example, by connecting the negative supply rail of operational amplifier OA1 to the input of current mirror CM1, an absolute-value precision peak detector is realised.

In most conventional peak-detector designs the common cause of output 'droop' when the circuit is in its hold mode, is the input bias current requirement of the operational amplifiers. However, with the new topology these effects are nulled during the initial setting up of the circuit, as previously described. Some, output droop will be caused by capacitor discharge through the output impedances of the current mirrors. For this reason, high output-impedance current mirrors, such as the improved Wilson [18] are preferable.

8 Discussion and conclusion

A novel application of operational-amplifier supply-current sensing has been used to provide wide-band pre-

cision rectification. Results have shown that a more accurate and linear transfer performance can be obtained over a wider bandwidth with this new rectifying circuit that with conventional circuits employing operational amplifiers and diodes. Results also indicate that operational amplifiers with low supply bias currents are preferable in these designs.

Application of this rectifying scheme in the design of high-performance precision peak-detection has also been described. The advantages of this new design over conventional precision peak detectors is the circuit simplicity and low cost required to provide high performance.

Finally, although constructed from transistor arrays and conventional operational amplifiers, the circuits discussed are all fully compatible with monolithic process technology and could be realised in integrated-circuit form.

9 References

1 GRAEME, J.G., TOBEY, G.E., and HUELSMAN, L.P.: 'Operational amplifiers, design and application'. (McGraw-Hill, 1971), p. 245
2 ROBERGE, J.K.: 'Operational amplifiers: theory and practice'. (Wiley, 1975), Chap. 11, pp. 458–460
3 ANTONIOU, A.: 'Design of precision rectifiers using operational amplifiers', *Proc. IEE*, 1974, **121**, (10), pp. 1041–1044
4 MEISKSIN, Z.H., and THACKRAY, P.C.: 'Electronic design with off-the-shelf integrated circuits' (Parker, 1980), Chap. 6, pp. 209–216
5 GRAY, P.R., and MEYER, R.G.: 'Analysis and design of Analog integrated circuits' (Wiley, 1984, 2nd edn.), Chap. 10, pp. 584–590
6 BARKER, R.W.J., and HART, B.L.: 'Versatile precision full-wave rectifier', *Electron. Lett.*, 1977, **13**, pp. 143–144
7 POOKAIYAUDOM, S., WATANACHAIPRATEEP, C., and DEJHAN, K.: 'A single-transistor full-wave rectifier', *Proc. IEEE*, 1979, **67**, (4), pp. 687–688
8 WAYNE, K.: 'A low cost rectifying amplifier and peak detector', *Electron. Eng.*, 1979, **51**, (631), pp. 28–29
9 RAO, M.K.N., and HASLETT, J.W.: 'Class AB bipolar voltage to current converter', *Electron. Lett.*, 1978, **14**, pp. 762–764
10 HASLETT, J.W., and RAO, M.K.N.: 'A high quality controlled current source', *IEEE Trans.*, 1979, **IM-28**, pp. 132–140
11 HART, B.L., and BARKER, R.W.J.: 'Universal operational-amplifier converter technique using supply current sensing', *Electron. Lett.*, 1979, **15**, pp. 496–497
12 WILSON, B.: 'Low distortion feedback voltage-current conversion technique', *ibid.*, 1981, **17**, pp. 157–159
13 WILSON, B.: 'A low-distortion bipolar feedback current amplifier technique', *Proc. IEEE*, 1981, **69**, pp. 1514–1515
14 LIDGEY, F.J., and TOUMAZOU, C.: 'Accurate current follower', *Electron & Wireless World*, 1985, **91**, (1590), pp. 17–19
15 WILSON, B.: 'High-performance current conveyor implementation', *Electron. Lett.*, 1984, **20**, pp. 990–991
16 TOUMAZOU, C., and LIDGEY, F.J.: 'Floating-impedance converters using current conveyors', *Electron. Lett.*, 1985, **21**, pp. 640–642
17 WILSON, B.: 'Floating FDNR employing a new CCII — conveyor implementation', *Electron. Lett.*, 1985, **21**, pp. 996–997
18 HART, B.L., and BARKER, R.W.J.: 'D.C. matching errors in the Wilson current source', *Electron. Lett.*, 1976, **12**, pp. 389–390
19 GRAEME, J.: 'Getting inside a peak detector to make it do the job', *Electron. Int.*, 1974, **74**, (24), pp. 145–149
20 FABRE, A.: 'Dual translinear voltage/current converter', *Electron. Lett.*, 1983, **19**, pp. 1030–1031
21 GILBERT, B.: 'Translinear circuits: A proposed classification', *ibid.*, 1975, **19**, pp. 14–16

10 Appendix

10.1 Theoretical evaluation of rectifier operation

A typical diagram of the basic class-AB push-pull output stage of an operational amplifier is shown in Fig. 8.

Current I_s is the DC bias current provided from a constant current source, which supplies the bias for diode-connected transistors Q_C and Q_D, and hence biases output transistors Q_A and Q_B in the forward active region. Input current I_{in} is in effect the operational amplifier's feedback current, approximately equal to V_{in}/R in the rectifier circuits of Fig. 2.

The circuit of Fig. 8 is a good approximation of a dual translinear loop [20] comprising transistors Q_A to Q_D.

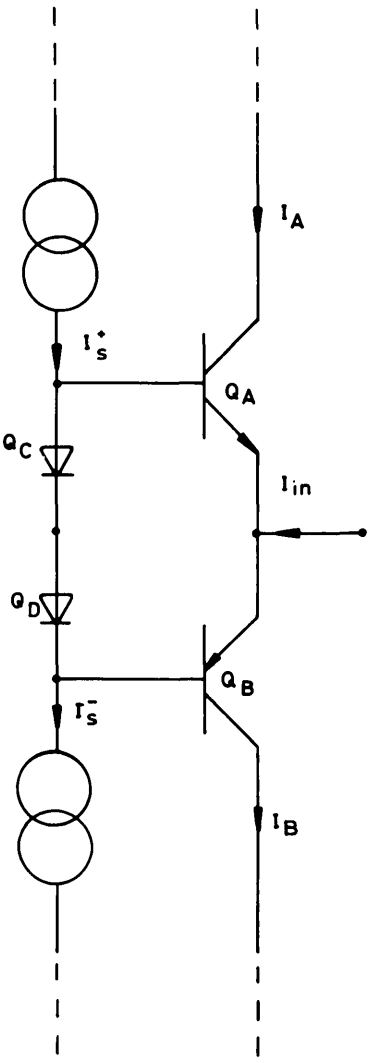

Fig. 8 *Typical class AB output stage*
$I_s^+ \simeq I_s^- \simeq I_s$

By application of the translinear circuit principle [21] around the loop Q_A to Q_B, it can be shown that

$$I_s^2 \simeq I_A I_B \tag{2}$$

When the input signal $I_{in} = 0$ it follows that: $I_A = I_B = I_s$.

However, it is of interest to examine what happens when I_{in} is nonzero and

$$I_B = I_A + I_{in} \tag{3}$$

From eqns. 1 and 2 we can solve for I_B and I_A and, hence

$$I_B \simeq I_{in}/2 + I_s[(I_{in}/2I_s)^2 + 1]^{1/2} \tag{4}$$

$$I_A \simeq -I_{in}/2 + I_s[(I_{in}/2I_s^2 + 1]^{1/2} \tag{5}$$

From eqns. 4 and 5 it can be seen that if $|I_{in}| \ll I_s$, then these equations reduce to

$$I_A \simeq I_s - I_{in}/2$$

$$I_B \simeq I_s + I_{in}/2$$

and the circuit's operating mode can be regarded as class A only.

If, however, $|I_{in}| \gg I_s$, the circuit will operate in a class-B mode and, therefore

$$I_A \simeq 0$$

and

$$I_B \simeq I_{in}$$

It is of interest to examine and quantify the nonlinear distribution of I_{in} in I_A and I_B, between these two extremes. I_A and I_B can be rewritten as

$$I_A = I_s - \delta I_{in} \quad (6)$$

$$I_B = I_s + (1 - \delta) I_{in} \quad (7)$$

where δ is the input-current distribution factor.

By equating eqns. 6 to 5 or eqns. 7 to 4 it can be shown that

$$\delta \simeq \tfrac{1}{2} - I_s/I_{in}[((I_{in}/2I_s)^2 + 1)^{1/2} - 1] \quad (8)$$

10.2 Experimental measurements of I_s and δ

The circuit of Fig. 9 was adopted as an experimental test circuit for measurements of I_s and δ for several different

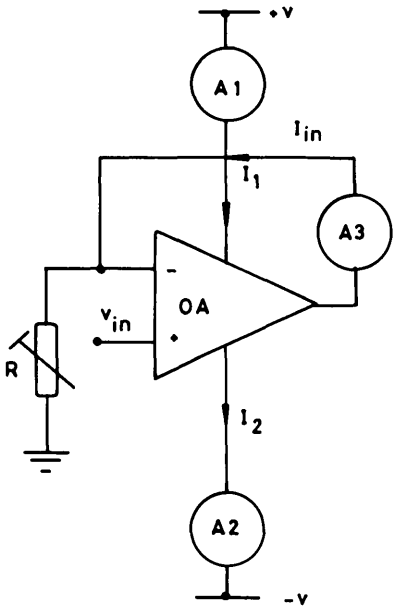

Fig. 9 *Experimental test set-up: I_s and δ measurements*

operational amplifiers. The input current $I_{in} = V_{in}/R$ was measured with ammeter A3 and operational amplifier supply currents I_1 and I_2 measured with ammeters A1 and A2 respectively.

10.2.1 Experimental procedure: (i) *I_s measurement.* Initially, input current I_{in} was set equal to zero and steady bias currents I_1 and I_2 denoted by I_{10} and I_{20} were measured. I_{in} was increased until bias current I_1 reduced to an approximately constant value I_{1c}. This is the effect of transistor Q_A slowly switching off and I_s^+ is given by

$$I_s^+ \simeq I_{10} - I_{1c} \quad (9)$$

Note that eqn. 9 assumes $I_A \simeq I_s^+$ for $I_{in} = 0$. As a test to check whether equal I_s is flowing through both positive and negative supply rails, a similar procedure can be adopted for I_s^- measurement with now $I_{in} < 0$. In this case

$$I_s^- \simeq I_{20} - I_{2c} \quad (10)$$

eqn. 10 also assumes $I_B \simeq I_s^-$ for $I_{in} = 0$.

The measurements confirm the expected result that $I_s^+ = I_s^- = I_s$.

(ii) *δ measurement.* Rearranging for δ in eqns. 6 and 7 then

$$\delta = [(I_s - I_A)/I_{in}] = 1 + [(I_s - I_B)/I_{in}] \quad (11)$$

I_A can be measured as $\simeq [I_1 - I_{1c}]$ and $I_B \simeq [I_2 - I_{2c}]$.

Substitution of I_A and I_B together with I_s from eqns. 9 and 10, into 11 yields

$$\delta \simeq [(I_{10} - I_1)/I_{in}] \simeq [1 + (I_{20} - I_2)/I_{in})/I_{in}] \quad (12)$$

10.3 Experimental results

For the LM741 operational amplifier, I_s was measured to be 0.254 mA and supply bias current $I_{10} = I_{20}$ measured to be 0.884 mA. For the LF441 operational amplifier I_s was 0.036 mA and $I_{10} = I_{20} \simeq 0.143$ mA.

Graphs of the current distribution factor δ against input current I_{in} for both operational amplifiers, were plotted from experimental values obtained from eqn. 12, and theoretical values obtained from eqn. 8, as shown in Fig. 10.

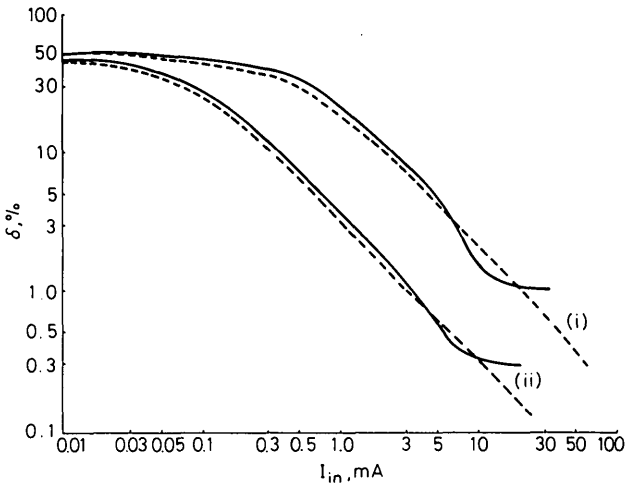

Fig. 10 *Graphs of current distribution factor δ% against input current I_{in}*
(i) LM741 operational amplifier
(ii) LF441 operational amplifier
——— experimental
- - - - theoretical

From the graphs it can be seen that good correlation for both operational amplifiers exists between theoretical values of δ and those obtained experimentally.

The graphs also indicate the expected wider distribution of input current between the operational amplifier's supply leads in the case of the larger supply current LM741 operational amplifier. For example, for a value of $I_{in} \simeq 1$ mA, in the case of the LM741 operational amplifier approximately 30% of the input current is drawn by the positive supply rail and 70% by the negative supply rail. However, for the LF441 operational amplifier only about 5% of the input current is drawn by the positive supply rail, the remaining 95% being drawn by the negative supply rail. It is this small amount of conduction in the opposite direction to the rectifier's main signal path that is responsible for the curvature at low input-current levels as seen in the transfer characteristics of Fig. 3. Optimum rectifying performance is, therefore, provided if the effects of δ are minimised. This is achieved by driving the operational amplifier near to maximum output, as indicated by the graphs of Fig. 10 and implied by the relation, expr. 1, in Section 4 of this paper.

Christopher Toumazou was born in 1961. He received his BSc in engineering from Oxford Polytechnic in 1983. From September 1983 to August 1986 he worked on novel current-mode analogue amplifier designs at Oxford Polytechnic and was awarded a PhD for this work in October 1986. At present he is a research fellow at Imperial College in the Department of Electrical Engineering, where he is engaged in research and development on switched-capacitor filters.

John Lidgey was born in 1947. He received his BSc in applied physics from South Bank Polytechnic in 1969 and his PhD in microwave electronics from the University of Surrey in 1973. From 1974 to 1978 he was a lecturer in electronics at the University of Newcastle in Australia. In 1978 he joined the Department of Engineering at Oxford Polytechnic where he is currently principal lecturer in electronics. His main teaching and research interests are in the areas of analogue circuit design, and in addition he is actively engaged in electronics consultancy.